NASA Contractor Report

Electromagnetic Scattering from a Rectangular Cavity Recessed in a 3D Conducting Surface

M. D. Deshpande
ViGYAN Inc., Hampton, VA. 23681

C. J. Reddy
Hampton University, Hampton, VA. 23666

Contract NAS1-19341

October 1995

National Aeronautics and
Space Administration
Langley Research Center
Hampton, Virginia 23681-0001

Contents

List of Tables

List of Figures

.

List of Symbols

a,b,c	x-, y-, and z-dimensions of rectangular cavity
$A_{n\theta}, A_{n\varphi}$	θ, φ components of magnetic vector potential due to $\vec{B}_n$
A^+, A^-	areas of D_n^+ and D_n^- triangles
$\vec{A}$	magnetic vector potential
a_p	complex modal amplitude of p^{th} forward travelling mode
b_p	complex modal amplitude of p^{th} backward travelling mode
$\vec{B}_n(\vec{r}')$	vector basis function for triangular subdomain
$[C]$, $[D]$, $[P]$, $[Q]$	matrices resulting from MoM method
$c_{n'n}$	$(n', n)^{th}$ element of matrix $[C]$
D_n^+, D_n^-	two triangles associated with n^{th} common edge
$d_{n', m}$	$(n', m)^{th}$ element of matrix $[D]$
$\vec{e}_p, \vec{h}_p$	rectangular waveguide vector modal functions for pth mode
$\vec{E}_i$	transverse electric field vector inside cavity
$\vec{E}_{in}$	incident electric field vector
$E_{\theta_i}, E_{\varphi_i}$	θ, φ components of incident electric field
E_{xi}, E_{yi}, E_{zi}	x-, y-, and z-components of incident electric field
$\lvert\vec{E}_i\rvert$	magnitude of incident electric field
$\vec{E}_s(\vec{m}_a)$	scattered electric field vector due to $\vec{m}_a$
$\vec{E}_s(\vec{j})$	scattered electric field vector due to $\vec{j}$
$E_{s\theta}, E_{s\varphi}$	θ, φ components of scattered electric far field
$\vec{F}$	electric vector potential
$F_{m\theta}, F_{m\varphi}$	θ, φ components of electric vector potential due to $\vec{B}_m$
$\vec{H}_i$	transverse magnetic field vector inside cavity
$\vec{H}_s(\vec{j})$	scattered magnetic field vector due to $\vec{j}$
$\vec{H}_s(\vec{m}_a)$	scattered magnetic field vector due to $\vec{m}_a$

$\vec{H}_{in}$	incident magnetic field
$\vec{j}$	electric surface current density
$\vec{j}\big\rvert_A$	electric surface current density over aperture
j	$=\sqrt{-1}$
k_0	free-space wave number
k	$= k_0\sqrt{\varepsilon_r\mu_r}$
k_x	$(m\pi)/a$ propagation constants along x-direction inside cavity
k_y	$(n\pi)/b$ propagation constants along y-direction inside cavity
$\vec{k}_i$	propagation vector along incidence direction
L	length of cavity
l_n	length of n^{th} edge
$\vec{m}_a$	magnetic surface current density
m, n	integer associated with triangular subdomains
M	total number of triangular elements on aperture
N	total number of triangular elements on 3D surface
p	integer, waveguide modal index
$p_{m', n}$	$(m', n)^{th}$ element of matrix $[P]$
$q_{m', m}$	$(m', m)^{th}$ element of matrix $[Q]$
$\vec{r}_1, \vec{r}_2$	position vectors of vertices opposite the n^{th} edge
$\vec{r}$	position vector of field point
$\vec{r}'$	position vector of source point
S_a	cavity aperture surface
S_c	surface area over which $\vec{j}$ exist
T_n, Γ_m	complex constants
$[T], [\Gamma], [U], [V]$	column matrices
$u_{n'}$	$(n')^{th}$ element of column matrix $[U]$
$v_{m'}$	$(m')^{th}$ element of column matrix $[V]$
$\hat{x}, \hat{y}, \hat{z}$	unit vector along the x-, y-, and z-axis, respectively

γ_p	propagation constant of p^{th} mode of cavity
θ_i, φ_i	plane wave incident angle in degrees
$\hat{\theta}_i$, $\hat{\varphi}_i$	unit vectors
α_0	angle in degrees
η_0	free-space impedance
ε_0, μ_0	permittivity and permeability of free-space
$\sigma_{\theta\theta}$	H co-polarized radar cross section pattern
$\sigma_{\varphi\varphi}$	E co-polarized radar cross section pattern
$\sigma_{\theta\varphi}$, $\sigma_{\varphi\theta}$	cross polarized radar cross section pattern
FEM-MoM	finite element method_ method of moments
ME-MoM	modal expansion_method of moments
EM	electromagnetic
EFIE	electric field integral equation
3D	three dimensional
RCS	radar cross section

Abstract

The problem of electromagnetic (EM) scattering from an aperture backed by a rectangular cavity recessed in a 3D conducting body is analyzed using the coupled field integral equation approach. Using the free-space Green's function, EM fields scattered outside the cavity are determined in terms of 1) an equivalent electric surface current density flowing on the 3D conducting surface of the object including the cavity aperture and 2) an equivalent magnetic surface current density flowing over the aperture only. The EM fields inside the cavity are determined using the waveguide modal expansion functions. Making the total tangential electric and magnetic fields across the aperture continuous and subjecting the total tangential electric field on the outer conducting 3D surface of the object to zero, a set of coupled integral equations is obtained. The equivalent electric and magnetic surface currents are then obtained by solving the coupled integral equation using the Method of Moments (MoM). The numerical results on scattering from rectangular cavities embedded in various 3-D objects are compared with the results obtained by other numerical techniques.

1. INTRODUCTION

Electromagnetic scattering characteristic of metallic cavities is useful in studying radar cross section and electromagnetic penetration properties of objects consisting of these cavities as substructures. A large amount of analytical work has been done to characterize these cavity structures. A few references, but not a complete list, are given in [1- 8]. However, in these and similar work, it is assumed that the aperture backed by a cavity is in an infinite flat ground plane. For a characterization of an aperture formed by a cavity recessed in a finite gound plane or no ground plane, the asymptotic techniques described in [9-11] may be used. However, these asymptotic techniques are applicable when the frequency is high or when the cavities are large in size compared to the operating wavelength. For cavities with size comparable with a wavelength, a rigorous integral equation formulation has been used to analyze cylindrical circular cavities [12-13]. However, the approach described in [12-13] uses entire domain expansion functions to represent surface current density and hence is limited to only cylindrical circular cylinders. A need, therefore, exists to develop general analytical tools to determine low frequency electromagnetic characteristics of open-ended waveguide cavities without a flang or recessed in 3D counducting surface.

In this paper the problem of EM scattering of plane waves by a cylindrical cavity recessed in a 3D metallic object is studied. Using the equivalence principle, the electromagnetic field scattered outside the object is determined using free space Green's function and the equivalent electric and magnetic surface currents assumed to be present on the outer surface of the object. The equivalent electric surface current is assumed to be flowing over the complete 3D surface including the aperture and the equivalent magnetic surface current is assumed to be flowing over only aperture. The field inside the cavity are obtained using waveguide modal expansion functions. Making the total tangential electric and magnetic fields across the aperture continuous and the total tangential electric field zero over the conducting surface only, a set of coupled integral equations is obtained. Expanding the surface currents in triangular subdomain functions [14] and using the Method of Moments, the coupled integral equations are reduced to algebric equations which are solved for the surface current densities. From the surface currents the radar cross sections of these cavities recessed in an arbitrarily shaped conducting objects are determined. For future reference, this method is refered to as Modal Expansion and Method of Moments (ME-MoM).

The remainder of report is organized as follows. The formulation of the problem in terms of coupled integral equations using surface equivalence principle is developed in section 2. Numerical results on radar cross section of open-ended rectangular cavities recessed in a rectangular and finite circular cylinder are presented in section 3. Comparison of the numerical results obtained by the present method with other numerical techniques is also presented in section 3. The advantages and limitations of the present formulation are discussed in section 4.

2. THEORY

Consider a time harmonic electromagnetic plane wave incident on a 3D conducting object with an aperture backed by a rectangular cavity as shown in figure 1. The cavity is formed by a shorting plate at z = -L. To facilitate the solution of the problem, the equivalence principle is applied by using the equivalent surface currents as shown in figure 2. For determining the fields outside the cavity (exterior problem), we consider the equivalent currents $\vec{j}$ and $\vec{m}_a$ radiating in free space. The electromagnetic field inside the cavity (interior problem) is obtained using modal expansion.

2.1 Interior Problem:

The transverse components of fields inside the cavity may be obtained using the procedure given in [15]. Expressing the transverse electric and magnetic fields in terms of vector modal functions and satisfying the boundary conditions, the fields inside the cavity may be written as

.

$$\vec{E}_i = \sum_{p=0}^{\infty}\left(\frac{j}{Y_p}\cdot\frac{Sin\,(\gamma_p\,(z+L)\,)}{Cos\,(\gamma_p L)}\right)\vec{e}_p\,(x,y)\cdot\iint_{S_a}\left(\vec{j}\big|_A\cdot\vec{e}_p\,(x,y)\right)ds \qquad (1)$$

$$\vec{H}_i = -\sum_{p=0}^{\infty} \frac{Cos(\gamma_p(z+L))}{Cos(\gamma_p L)} \vec{h}_p(x,y) \cdot \iint_{S_a} \left(\vec{j}\big|_A \cdot \vec{e}_p(x,y) \right) ds \tag{2}$$

where γ_p is the propagation constant, equal to $\sqrt{k^2 - k_x^2 - k_y^2}$, $k^2 = k_0^2 \varepsilon_r \mu_r$, (ε_r and μ_r are relative permittivity and permeability of medium inside the cavity), Y_p is the modal admittance, $\vec{e}_p(x,y)$ and $\vec{h}_p(x,y)$ are the vector modal functions as defined in [15], $\vec{j}\big|_A = \hat{z} \times \vec{H}_t$, $\vec{H}_t$ being the tangential magnetic field over the aperture, and $\vec{e}_p(x,y) = \vec{h}_p(x,y) \times \hat{z}$, $\hat{z}$ being the unit vector along the z-axis.

If the 3D surface is divided into triangular subdomains, the electric current over the surface of the 3D object including the aperture may be expressed in terms of triangular basis functions as [14]

$$\vec{j}(x,y,z) = \sum_{n=1}^{N} T_n \vec{B}_n(\vec{r}') \tag{3}$$

where T_n is the amplitude of electric current normal to the n^{th} edge, $\vec{B}_n(\vec{r}')$ is the vector basis fuction associated with n^{th} edge, and N is the number of non-boundary edges on the surface of the object. The expression for basis function is given by [14]

$$\vec{B}_n\left(\vec{r}_i\right)\Big| = \begin{pmatrix} \dfrac{l_n}{2\,A^+}\left(\vec{r}' - \vec{r}_1\right) \text{, when } \vec{r}' \text{ in } D_n^+ \\ \dfrac{l_n}{2\,A^-}\left(\vec{r}_2 - \vec{r}'\right) \text{, when } \vec{r}' \text{ in } D_n^- \end{pmatrix} \tag{4}$$

where D_n^+ and D_n^- are the two triangles with the n^{th} common edge, A^+ and A^- are the areas of D_n^+ and D_n^- triangles, respectively, and $\vec{r}_1$ and $\vec{r}_2$ are position vectors of vertices opposite the the n^{th} common edge of D_n^+ and D_n^- triangles, respectively. Likewise the magnetic current over the aperture may be written as

$$\overrightarrow{m_a}(x, y, z) = \sum_{m=1}^{M} \Gamma_m \vec{B}_m(\vec{r}') \tag{5}$$

where Γ_m is amplitude of magnetic current normal to the m^{th} edge, and M is the number of non-boudary edges over the aperture. Substituting (3) in equations (1) and (2), the total fields inside the cavity are obtained as

$$\vec{E}_i = \sum_{n=1}^{N} T_n \cdot \left\{ \sum_{p=0}^{\infty} \left(\frac{j}{Y_p} \cdot \frac{Sin(\gamma_p(z+L))}{Cos(\gamma_p L)} \right) \vec{e}(x, y) \cdot \iint_{S_a} \left(\overrightarrow{B_n} \cdot \overrightarrow{e_p}(x, y) \right) ds \right\} \tag{6}$$

$$\vec{H}_i = \sum_{n=1}^{N} T_n \cdot \left\{ -\sum_{p=0}^{\infty} \frac{Cos(\gamma_p(z+L))}{Cos(\gamma_p L)} \vec{h}_p(x, y) \cdot \iint_{S_a} \left(\overrightarrow{B_n} \cdot \overrightarrow{e_p}(x, y) \right) ds \right\} \tag{7}$$

2.2 Electromagnetic Field in Exterior Part:

In the exterior part, the total electromagnetic field is obtained by superposing the scattered field due to $\vec{j}$ and $\vec{m}_a$, and the incident field.

2.2.1 Incident Field:

The incident field with time variation $e^{j\omega t}$ may be written as

$$\vec{E}_{in} = \left(\hat{\theta}_i E_{\theta_i} + \hat{\phi}_i E_{\phi_i} \right) e^{-j\vec{k}_i \bullet \vec{r}} \tag{8}$$

where $\vec{k}_i = -k_0 [\hat{x} Cos(\phi_i) Sin(\theta_i) + \hat{y} Sin(\phi_i) Sin(\theta_i) + \hat{z} Cos(\theta_i)]$, $\vec{r} = \hat{x}x + \hat{y}y + \hat{z}z$, $E_{\theta_i} = |\vec{E}_i| Cos(\alpha_0)$, and $E_{\phi_i} = |\vec{E}_i| Sin(\alpha_0)$, and k_0 being the free-space wave number. With reference to figure 1, $\alpha_0 = 0$ corresponds to H-polarization and $\alpha_0 = 90^0$ corresponds to E-polarization. From equation (8), the x-, y-, and z-components of the incident field may be written, respectively, as

$$E_{xi} = E_{\theta_i} Cos(\theta_i) Cos(\phi_i) - E_{\phi_i} Sin(\phi_i) \tag{9}$$

$$E_{yi} = E_{\theta_i} Cos(\theta_i) Sin(\phi_i) + E_{\phi_i} Cos(\phi_i) \tag{10}$$

$$E_{zi} = -E_{\theta_i} Sin(\theta_i) \tag{11}$$

The corresponding magnetic field components are obtained through

$$\vec{H}_{in} = \frac{1}{k_0 \eta_0} \vec{k}_i \times \vec{E}_{in} \tag{12}$$

where η_0 is the free-space impedance. The incident field with $E_{\theta_i} \neq 0$ and $E_{\phi_i} = 0$ is called H-polarized wave and $E_{\theta_i} = 0$ and $E_{\phi_i} \neq 0$ is called the E-polarized wave.

2.2.2 Scattered Field:

The scattered field outside the cavity due to $\vec{j}$ and $\vec{m}_a$ may be obtained through vector electric and magnetic potentials as

$$\vec{E}_s(\vec{j}) = -j\omega\vec{A} - \frac{j}{\omega\mu_0\varepsilon_0} \nabla\nabla \bullet \vec{A} \tag{13}$$

$$\vec{H}_s(\vec{j}) = \frac{1}{\mu_0} \nabla \times \vec{A} \tag{14}$$

$$\vec{E}_s(\overrightarrow{m_a}) = \left(-\frac{1}{\varepsilon_0}\right) \nabla \times \vec{F} \tag{15}$$

$$\vec{H}_s(\overrightarrow{m_a}) = -j\omega\vec{F} - \frac{j}{\omega\mu_0\varepsilon_0} \nabla\nabla \bullet \vec{F} \tag{16}$$

where the electric and magnetic vector potentials are given by

$$\vec{F}(\vec{m}_a) = \frac{\varepsilon_0}{4\pi} \cdot \iint_{S_a} \left(\vec{m}_a \cdot \frac{e^{-jk_0(\vec{r} - \vec{r}')}}{|\vec{r} - \vec{r}'|} \right) ds \tag{17}$$

$$\vec{A}\left(\vec{j}\right) = \frac{\mu_0}{4\pi} \cdot \iint_{S_a} \left(\vec{j} \cdot \frac{e^{-jk_0(\vec{r} - \vec{r}')}}{|\vec{r} - \vec{r}'|} \right) ds \tag{18}$$

ε_0, and μ_0 are the permittivity and permeability, respectively, of free-space, and $\vec{r}$ and $\vec{r}'$ are the coordinates of the field and source points, respectively. Using equations (3) and (5), the total scattered electric and magnetic fields may be written as

$$\vec{E}_s = \sum_{n=1}^{N} T_n \cdot \left(-j\omega \vec{A}_n - \frac{j}{\omega\mu_0\varepsilon_0} \nabla\nabla \bullet \vec{A}_n \right) + \sum_{m=1}^{M} \Gamma_m \cdot \frac{1}{\varepsilon_0} \cdot \nabla \times \vec{F}_m \tag{19}$$

$$\vec{H}_s = \sum_{n=1}^{N} T_n \frac{1}{\mu_0} \nabla \times \vec{A}_n + \sum_{m=1}^{M} \Gamma_m \left(-j\omega \vec{F}_m - \frac{j}{\omega\mu_0\varepsilon_0} \nabla\nabla \bullet \vec{F}_m \right) \tag{20}$$

where N is total number of non-boundary edges over the 3D body including the aperture area, and M is total number of non-boundary edges over the aperture area only. $\vec{A}_n$ and $\vec{F}_m$ appearing in (19) and (20) are obtained from equations (17) and (18), respectively, by replacing $\vec{j}$ by $\vec{B}_n$ in (17) and $\vec{m}_a$ by $\vec{B}_m$ in (18).

2.3 Coupled Integral Equations:

Making the total tangential fields across the aperture continuous and the total tangential electric field on the conducting surface of the object to zero we get the following coupled integral equations:

$$\left[\sum_{n=1}^{N} T_n \cdot \left(-j\omega \vec{A}_n - \frac{j}{\omega\mu_0\varepsilon_0} \nabla\nabla \bullet \vec{A}_n \right) + \sum_{m=1}^{M} \Gamma_m \cdot \frac{1}{\varepsilon_0} \cdot \nabla \times \vec{F}_m + \vec{E}_{in} \right]_{\tan} =$$

$$\sum_{n=1}^{N} T_n \cdot \left\{ \sum_{p=0}^{\infty} \left(\frac{j}{Y_p} \cdot \frac{Sin(\gamma_p(z+L))}{Cos(\gamma_p L)} \right) \vec{e}(x,y) \cdot \iint_{S_a} \left(\vec{B}_n \cdot \vec{e}_p(x,y) \right) ds \right\} \tag{21}$$

$$\left[\sum_{n=1}^{N} T_n \frac{1}{\mu_0} \nabla\times\vec{A}_n + \sum_{m=1}^{M} \Gamma_m \left(-j\omega\vec{F}_m - \frac{j}{\omega\mu_0\varepsilon_0} \nabla\nabla\bullet\vec{F}_m \right) + \vec{H}_{in} \right]_{\tan} =$$

$$- \sum_{n=1}^{N} T_n \cdot \left\{ \sum_{p=0}^{\infty} \frac{Cos(\gamma_p (z+L))}{Cos(\gamma_p L)} \vec{h}_p(x,y) \cdot \iint_{S_a} \left(\vec{B}_n \cdot \vec{e}_p(x,y) \right) ds \right\} \qquad (22)$$

The integral equations given in (21) and (22) may be reduced to a set of algebric equations by application of the Method of Moments. By selecting $\vec{B}_{n'}$ with $n'=1,2,...N$ as testing functions for equation (21) and $\vec{B}_{m'}$ with $m'=1,2....M$ as testing functions for the equation (22), the application of the Method of Moments results in the following matrix equation:

$$\begin{bmatrix} [C] & [D] \\ [P] & [Q] \end{bmatrix} \cdot \begin{bmatrix} [T] \\ [\Gamma] \end{bmatrix} = \begin{bmatrix} [U] \\ [V] \end{bmatrix} \qquad (23)$$

The elements of matrices $[C]$, $[D]$, $[P]$, and $[Q]$ are given by

$$c_{n'n} = \iint_{D_{n'}} \vec{B}_{n'} \bullet \left(-j\omega\vec{A}_n - \frac{j}{\omega\mu\varepsilon} \nabla\nabla\bullet\vec{A}_n \right) ds$$

$$- \left\{ \sum_{p=0}^{\infty} \frac{j}{Y_p} \cdot \frac{Sin(\gamma_p(L))}{Cos(\gamma_p L)} \left(\iint_{D_{n'}} \left(\vec{B}_{n'} \bullet \vec{e}_p(x,y) \right) ds \cdot \iint_{D_n} \left(\left(\vec{B}_n \bullet \vec{e}_p(x,y) \right) \right) ds \right) \right\} \qquad (24)$$

$$d_{n'm} = \iint_{D_{n'}} \vec{B}_{n'} \bullet \frac{1}{\varepsilon} \cdot \nabla\times\vec{F}_m ds \qquad (25)$$

$$p_{m'n} = \int\limits_{D_{m'}}\int \vec{B}_{m'} \bullet \frac{1}{\varepsilon} \cdot \nabla\times\vec{A}_n ds$$

$$+ \sum_{n=1}^{N} T_n \cdot \left\{ \sum_{p=0}^{\infty} \frac{Cos(\gamma_p(z+L))}{Cos(\gamma_p L)} \int\limits_{D_{m'}}\int \left(\overrightarrow{B_{m'}} \bullet \vec{h}_p(x,y) \right) ds \cdot \int\limits_{D_n}\int \left(\vec{B}_n \cdot \vec{e}_p(x,y) \right) ds \right\} \quad (26)$$

$$q_{m'm} = \int\limits_{D_{m'}}\int \vec{B}_{m'} \bullet \left(-j\omega\vec{F}_m - \frac{j}{\omega\mu\varepsilon}\nabla\nabla\bullet\vec{F}_m \right) ds$$

The elements of column matrices $[U]$ and $[V]$ are given by

$$u_{n'} = -\int\limits_{D_{n'}}\int \vec{E}_{in} \bullet \vec{B}_{n'} ds \quad (27)$$

$$v_{m'} = -\int\limits_{D_{m'}}\int \vec{H}_{in} \bullet \vec{B}_{m'} ds \quad (28)$$

In evaluating numerical values of expressions (24)-(28), numerical integration over the triangles are performed using thirteen point gauss quadrature formula [16]. For evaluation of self terms; i.e., when $n = n'$ or $m = m'$, closed form expressions for these expressions given in [17] are used. The unknown electric and magnetic current amplitudes obtained after solving the matrix equation (23) can be used to determine scattered far field using expression (19) and (20).

2.4 Scattered Far Field:

Using the far field approximation, the scattered electric far field may be obtained from equation (19) as

$$E_{s\theta} = -\sum_{n=1}^{N} T_n \cdot j\omega A_{n\theta} - \sum_{m=1}^{M} \Gamma_m jk_0 \cdot F_{m\phi} \quad (29)$$

$$E_{s\phi} = -\sum_{n=1}^{N} T_n \cdot j\omega A_{n\phi} + \sum_{m=1}^{M} \Gamma_m jk_0 \cdot F_{m\theta} \quad (30)$$

where $A_{n\theta}$, $A_{n\phi}$, $F_{m\theta}$, and $F_{m\phi}$ are given by

$$\vec{A}_n = \hat{\theta}A_{n\theta} + \hat{\phi}A_{n\phi} = \frac{e^{-jk_0 r}}{4\pi r}\iint_{S_n}\left(\vec{B}_n \cdot e^{jk_0 Sin(\theta)\,[x'Cos(\phi) + y'Sin(\phi)] + jk_0 z'Cos(\theta)}\right)ds_n \tag{31}$$

$$\vec{F}_m = \hat{\theta}F_{m\theta} + \hat{\phi}F_{m\phi} = \frac{e^{-jk_0 r}}{4\pi r}\iint_{S_m}\left(\vec{B}_m \cdot e^{jk_0 Sin(\theta)\,[x'Cos(\phi) + y'Sin(\phi)] + jk_0 z'Cos(\theta)}\right)ds_n \tag{32}$$

The copolarized radar cross section patterns of an aperture backed by a cavity in a 3D conducting surface can be obtained from

$$\sigma_{\theta\theta} = \lim_{r \to \infty} 4\pi r^2 \frac{|E_{s\theta}|^2}{|E_{\theta_i}|^2} \tag{33}$$

for H-polarized incidence and

$$\sigma_{\varphi\varphi} = \lim_{r \to \infty} 4\pi r^2 \frac{|E_{s\phi}|^2}{|E_{\phi_i}|^2} \tag{34}$$

for E-polarized incidence. The cross-polarized radar cross section pattern is obtained from

‘

$$\sigma_{\varphi\theta} = \sigma_{\theta\varphi} = \lim_{r \to \infty} 4\pi r^2 \frac{|E_{s\phi}|^2}{|E_{\theta_i}|^2} = \lim_{r \to \infty} 4\pi r^2 \frac{|E_{s\theta}|^2}{|E_{\varphi_i}|^2} \tag{35}$$

3. CODE IMPLEMENTATION

The coupled field integral equation approach to solve the problem of scattering from a rectangular waveguide embedded in a 3D conducting surface has been implemented through a code named scatt_reap_recav_3d (*scatt*ering from *re*ctangular *ap*erture backed by a *re*ctangular *cav*ity embedded in a *3d* conducting object).

For running the scatt_reap_recav_3d code, the given geometry is modelled using COSMOS/M. In using COSMOS/M, it is assumed that user is familiar with operation of COSMOS/M. All dimensions of 3D surface and rectangular cavity are normalized with respect to the operating wavelength.

The input variables must be defined in a file called **.in* before running *scatt_reap_recav_3d*. A sample of **.in* is given in Table 1.

Table 1: Description of*.*in* file

Variable	Description
*.MOD	Name of input file containing nodes and element information
output file name	Name of output file where output is stored
aa,bb	x- and y-dimensions of rectangular cavity in wavelength
al0	length of cavity in wavelength
ihigher	an integer, if zero only dominant mode in the cavity is considered. It also skips next line if “ ihigher “ is zero
ite, itm	integers, read only if “ ihigher” is not zero. ite is number of TE modes and itm is number of TM modes to be considered in the cavity
alpha	0 for H-polarization 90 for E-polarization

Table 1: Description of*.*in* file

Variable	Description
theta, phi	incident theta and phi angles in degrees
thinc, phinc	increments in theta and phi
die, emie	complex relative permittivity and permeability of medium inside the cavity

To demonstrate use of the code, the following examples are considered in this report

1) rectangular cavity without a ground plane

2) rectangular cavity embedded in a conducting cube

3) rectangular cavity embedded at the end of finite circular cylinder

4) rectangular cavity embedded in the curve surface of finite circular cylinder

3.1 EXAMPLE 1

To illustrate use of variables defined in Table I, a rectangular cavity shown in figure 3 is taken as an example. To generate *.MOD file for the geometry of figure 3 , *figure3.SES* file given in Table 1.1 is first run with COSMOS/M. The *.MOD file thus generated is named as *figure3.MOD*. The *figure3.in* file used for running the *scatt_reap_recav_3d* code is shown in Table 1.2 and a sample output of *scatt_reap_recav_3d* shown in **Table 1.3.**

Table 1.1 Listing of *figure3.SES*

```
C*  COSMOS/M      Geostar V1.70
C*  Problem : cube          Date : 11-29-94  Time :  8:47: 4
C*
PT 1 0 0 0
PT 2 -0.15 -0.15 0
PT 3 0.15 -0.15 0
PT 4 0.15 0.15 0
```

```
PT 5 -0.15 0.15 0
PT 6 -0.15 -0.15 -0.2
PT 7 0.15 -0.15 -0.2
PT 8 0.15 0.15 -0.2
PT 9 -0.15 0.15 -0.2
SCALE 0
CRLINE 1 2 3
CRLINE 2 3 4
CRLINE 3 4 5
CRLINE 4 5 2
CRLINE 5 6 7
CRLINE 6 7 8
CRLINE 7 8 9
CRLINE 8 9 6
CRLINE 9 2 6
CRLINE 10 3 7
CRLINE 11 4 8
CRLINE 12 5 9
CT 1 0 0.06 4 1 2 3 4 0
CT 2 0 0.06 4 2 10 6 11 0 1
CT 3 0 0.06 4 6 7 8 5 0 1
CT 4 0 0.06 4 4 9 8 12 0 1
CT 5 0 0.06 4 1 10 5 9 0 1
CT 6 0 0.06 4 3 11 7 12 0 1
RG 1 1 1 0
RG 2 1 2 0
RG 3 1 3 0
RG 4 1 4 0
RG 5 1 5 0
RG 6 1 6 0
PH 1 RG 1 0.06 0.0001 1
MA_PH 1 1 1
PRG 1 1 1 1 1 4
NMERGE
NCOMPRESS
NTCR 1 1 1 1
NPCR 2 2 2 1
NJCR 3 3 3 1
QCR 4 4 4 1
```

Table 1.2 Listing of *figure3.in*

figure3.MOD	" Input file with node and element information"
figure3.out	" Output file with RCS as a function of look angle"
0.3,0.3	" x- and y- dimensions normalized with wavelength of rectangular cavity
0.2	length of cavity normalized with respect to wavelength

1	integer flag to consider higher order modes in the cavity
10	number of TE modes to be considered
10	number of TM modes to be considered
0	alpha = 0 for H-polarization
0.,0.	theta and phi incident angles in degrees
1.,0	increment in theta and phi in degrees
30.	frequency in GHz
(1.,0.),(1.,0.)	complex relative permittivity and permeability of medium inside cavity

Table 1.3 Listing of *figure3.out*

```
 X-dimension of WG =  0.3000000    wavelength
 Y-dimension of WG =  0.3000000    wavelength
 Length of WG cavity =  0.2000000    wavelength
 Number of waveguide modes =          20
 Number of Nodes Used =   128
 Number of Elements Used =      252
 Number of nonboundary edges =          378
 Number of nonboundary edges (aperture)       =           65
 Frequency in Ghz =    30.00000
alphatheta      phi         cross-pol(RCS)co-pol(RCS)
  0.0.          0.          -42.90524    0.1645633
  0.1.000000    0.          -42.87325    0.1629779
  0.2.000000    0.          -42.85700    0.1584223
  0.3.000000    0.          -42.85587    0.1508932
  0.4.000000    0.          -42.86822    0.1403691
  0.5.000000    0.          -42.89356    0.1268443
  0.6.000000    0.          -42.93044    0.1102918
  0.7.000000    0.          -42.97783    9.0677880E-02
  0.8.000000    0.          -43.03438    6.7987286E-02
  0.9.000000    0.          -43.09773    4.2179674E-02
  0.10.00000    0.          -43.16571    1.3209175E-02
 **********     ***         ********     ************
 **********     ***         ********     ************
   0.171.0000   0.          -49.14130    -0.9871500
  0.172.0000    0.          -49.60229    -0.9702910
  0.173.0000    0.          -50.03440    -0.9554753
  0.174.0000    0.          -50.42996    -0.9426595
  0.175.0000    0.          -50.78228    -0.9318268
  0.176.0000    0.          -51.08117    -0.9229562
  0.177.0000    0.          -51.32377    -0.9160256
  0.178.0000    0.          -51.50285    -0.9110218
  0.179.0000    0.          -51.61285    -0.9079247
  0.180.0000    0.          -51.65466    -0.9067491
```

3.2 EXAMPLE 2

A rectangular cavity embedded in a metal cube as shown in figure 4 is considered as a second example. The *.SES, *. in, and *. out files used to for the problem are shown in Tables 2.1, 2.2, and 2.3.

Table 2.1 Listing of *figure4.SES*

```
C*
C*  COSMOS/M      Geostar V1.70
C*  Problem : figur4          Date :  1-11-95  Time : 10:25:41
C*
PLANE Z 0 1
VIEW 0 0 1 0
PT 1 -0.25 -0.25 0
PT 2 0.25 -0.25 0
PT 3 0.25 0.25 0
PT 4 -0.25 0.25 0
SCALE 0
PT 5 -0.25 -0.25 -0.5
PT 6 0.25 -0.25 -0.5
PT 7 0.25 0.25 -0.5
PT 8 -0.25 0.25 -0.5
PT 9 -0.15 -0.15 0
PT 10 0.15 -0.15 0
PT 11 0.15 0.15 0
PT 12 -0.15 0.15 0
VIEW 1 1 1 0
SCALE 0
CRLINE 1 1 2
CRLINE 2 2 3
CRLINE 3 3 4
CRLINE 4 4 1
CRLINE 5 5 6
CRLINE 6 6 7
CRLINE 7 7 8
CRLINE 8 8 5
CRLINE 9 1 5
CRLINE 10 2 6
CRLINE 11 3 7
CRLINE 12 4 8
CRLINE 13 9 10
CRLINE 14 10 11
CRLINE 15 11 12
```

```
CRLINE 16 12 9
CLS 1
CT 1 0 0.07 4 1 2 3 4 0
CT 2 0 0.07 4 13 14 15 16 0
RG 1 2 1 2 0
RG 2 1 2 0
CT 3 0 0.07 4 2 10 6 11 0 1
RG 3 1 3 0
CT 4 0 0.07 4 3 11 7 12 0 1
RG 4 1 4 0
CT 5 0 0.07 4 4 9 8 12 0 1
RG 5 1 5 0
CT 6 0 0.07 4 1 10 5 9 0 1
RG 6 1 6 0
CT 7 0 0.07 4 5 6 7 8 0 1
RG 7 1 7 0
PH 1 RG 1 0.07 0.0001 1
MA_PH 1 1 1
PRG 2 1 2 1 1 4
NTCR 13 1 13 1
NPCR 14 2 14 1
NJCR 15 3 15 1
QCR 16 4 16 1
```

Table 2.2 Listing of *figure4.in*

figure4.MOD	" Input file with node and element information"
figure4.out	" Output file with RCS as a function of look angle"
0.3,0.3	" x- and y- dimensions normalized with wavelength of rectangular cavity
0.2	length of cavity normalized with respect to wavelength
1	integer flag to consider higher order modes in the cavity
30	number of TE modes to be considered
30	number of TM modes to be considered
0	alpha = 0 for H-polarization
0.,0.	theta and phi incident angles in degrees
1.,0	increment in theta and phi in degrees
30.	frequency in GHz
(1.,0.),(1.,0.)	complex relative permittivity and permeability of medium inside cavity

Table 2.3 Listing of *figure4.out*

```
 X-dimension of WG =  0.3000000    wavelength
 Y-dimension of WG =  0.3000000    wavelength
```

Length of WG cavity = 0.2000000 wavelength
Number of waveguide modes = 60
Number of Nodes Used = 152
Number of Elements Used = 300
Frequency in Ghz = 30.00000

alpha	theta	phi	cross-pol	co-pol
0.	0.	0.	-13.86164	3.597274
0.	1.000000	0.	-13.86652	3.586681
0.	2.000000	0.	-13.87791	3.557459
0.	3.000000	0.	-13.89583	3.509618
0.	4.000000	0.	-13.92023	3.443209
0.	5.000000	0.	-13.95116	3.358291
0.	6.000000	0.	-13.98853	3.254961
0.	7.000000	0.	-14.03238	3.133344
0.	8.000000	0.	-14.08267	2.993612
0.	9.000000	0.	-14.13940	2.836054
0.	10.00000	0.	-14.20255	2.660966
0.	11.00000	0.	-14.27210	2.468850
0.	12.00000	0.	-14.34806	2.260279
0.	13.00000	0.	-14.43036	2.036047
0.	14.00000	0.	-14.51905	1.797124
0.	15.00000	0.	-14.61407	1.544816
0.	16.00000	0.	-14.71538	1.280692
0.	17.00000	0.	-14.82301	1.006683
0.	18.00000	0.	-14.93689	0.7251824
0.	19.00000	0.	-15.05705	0.4389912
0.	20.00000	0.	-15.18342	0.1514122
0.	21.00000	0.	-15.31600	-0.1337813
0.	22.00000	0.	-15.45476	-0.4124082
0.	23.00000	0.	-15.59963	-0.6800060
0.	24.00000	0.	-15.75065	-0.9319531
0.	25.00000	0.	-15.90774	-1.163811
-	-------	--	--------	--------
-	-------	--	-------	--------
0.	170.0000	0.	-32.80526	2.489367
0.	171.0000	0.	-32.59278	2.690944
0.	172.0000	0.	-32.40409	2.870220
0.	173.0000	0.	-32.23733	3.027478
0.	174.0000	0.	-32.09236	3.163024
0.	175.0000	0.	-31.97046	3.277061
0.	176.0000	0.	-31.86998	3.369819
0.	177.0000	0.	-31.79082	3.441491
0.	178.0000	0.	-31.73413	3.492200
0.	179.0000	0.	-31.69735	3.522068
0.	180.0000	0.	-31.68309	3.531136

3.3 Example 3

In this example a rectangular aperture backed by a rectangular cavity placed at the one end of a finite circular cylinder as shown in figure 5 is considered. *. SES, *. in, and *. out files used for this problem are shown in Tables 3.1, 3.2, and 3.3, respectively**.**

Table 3.1 Listing of *figure5.SES*

```
C*
C*  COSMOS/M      Geostar V1.70
C*  Problem : figure5          Date :  1-25-95  Time : 15:52:43
C*
C* FILE temp1.SES 1 1 1 1
PLANE Z 0 1
VIEW 0 0 1 0
PT 1 0 0 0
PT 2 0.35 0.35 0
SCALE 0
CRPCIRC 1 1 2 0.494975 360 4
SCALE 0
SCALE 0
PT 6 0 0 -0.5
PT 7 0.35 0.35 -0.5
SCALE 0
VIEW 1 1 1 0
CRPCIRC 5 6 7 0.494975 360 4
PT 11 -0.15 -0.15 0
PT 12 0.15 -0.15 0
PT 13 0.15 0.15 0
PT 14 -0.15 0.15 0
CRLINE 9 2 7
CRLINE 10 3 8
CRLINE 11 4 9
CRLINE 12 5 10
CRLINE 13 11 12
CRLINE 14 12 13
CRLINE 15 13 14
CRLINE 16 14 11
CRLINE 17 12 5
CRLINE 18 13 2
CRLINE 19 14 3
CRLINE 20 11 4
```

```
SF4CR 1 3 17 13 20 0
SF4CR 2 17 4 18 14 0
SF4CR 3 18 1 19 15 0
SF4CR 4 19 2 20 16 0
SF4CR 5 13 14 15 16 0
SF4CR 6 1 9 5 10 0
SF4CR 7 10 6 11 2 0
SF4CR 8 11 3 12 7 0
SF4CR 9 12 8 9 4 0
SF4CR 10 5 6 7 8 0
PH 1 SF 1 0.1 0.0001 1
MA_PH 1 1 1
NTCR 13 1 13 1
NPCR 14 2 14 1
NJCR 15 3 15 1
QCR 16 4 16 1
PSF 5 1 5 1 1 1 4
NMERGE 1 831 1 0.0001 0 1 0
NCOMPRESS 1 831
```

Table 3.2 Listing of *figure5.in*

figure5.MOD	" Input file with node and element information"
figure5.out	" Output file with RCS as a function of look angle"
0.3,0.3	" x- and y- dimensions normalized with wavelength of rectangular cavity
0.2	length of cavity normalized with respect to wavelength
1	integer flag to consider higher order modes in the cavity
10	number of TE modes to be considered
10	number of TM modes to be considered
0	alpha = 0 for H-polarization (for E-polarization alpha =90)
0.,0.	theta and phi incident angles in degrees
1.,0	increment in theta and phi in degrees
30.	frequency in GHz
(1.,0.),(1.,0.)	complex relative permittivity and permeability of medium inside cavity

Table 3.3 Listing of *figure5.out*

```
X-dimension of WG =  0.3000000    wavelength
Y-dimension of WG =  0.3000000    wavelength
Length of WG cavity =  0.2000000    wavelength
Number of waveguide modes =         20
Number of Nodes Used =   831
Number of Elements Used =     1658
Frequency in Ghz =    30.00000
```

alpha	theta	phi	cross-pol	co-pol
0.	0.	0.	-5.916269	9.834730
0.	1.000000	0.	-5.920516	9.820421
0.	2.000000	0.	-5.933593	9.778456
0.	3.000000	0.	-5.955378	9.709249
0.	4.000000	0.	-5.985921	9.613455
0.	5.000000	0.	-6.025254	9.492058
0.	6.000000	0.	-6.073274	9.346359
0.	7.000000	0.	-6.129971	9.177999
0.	8.000000	0.	-6.195318	8.988997
0.	9.000000	0.	-6.269305	8.781787
0.	10.00000	0.	-6.351826	8.559145
0.	11.00000	0.	-6.442932	8.324296
0.	12.00000	0.	-6.542520	8.080740
0.	13.00000	0.	-6.650455	7.832253
--	-------	--	--------	-------
--	-------	--	-------	-------
0.	169.0000	0.	-33.84848	7.762480
0.	170.0000	0.	-33.33032	8.084915
0.	171.0000	0.	-32.86591	8.382092
0.	172.0000	0.	-32.45417	8.652040
0.	173.0000	0.	-32.09342	8.893197
0.	174.0000	0.	-31.78228	9.104296
0.	175.0000	0.	-31.52011	9.284355
0.	176.0000	0.	-31.30555	9.432592
0.	177.0000	0.	-31.13779	9.548450
0.	178.0000	0.	-31.01659	9.631517
0.	179.0000	0.	-30.94126	9.681516
0.	180.0000	0.	-30.91166	9.698285

3.4 Example 4

A rectangular aperture backed by a rectangular cavity and placed over the curved surface of a finite circular cylinder as shown in figure 6 is considered. *. SES, *. in, and *. out files used in this case are shown in Tables 4.1, 4.2, and 4.2, respectively**.**

Table 4.1 Listing of *figure6.SES*

```
C*
C*  COSMOS/M      Geostar V1.70
C*  Problem : figure6          Date :  1-26-95  Time :  8:10:19
```

```
C*
C* FILE temp1.SES 1 1 1 1
PLANE Z 0 1
VIEW 0 0 1 0
PT 1 0 0 0
PT 2 -0.35 -0.1505 0
PT 3 0.35 -0.1505 0
PT 4 0.35 0.1505 0
PT 5 -0.35 0.1505 0
PT 6 -0.35 -0.1505 0.1
PT 7 0.35 -0.1505 0.1
PT 8 0.35 0.1505 0.1
PT 9 -0.35 0.1505 0.1
SCALE 0
VIEW 1 1 1 0
PT 10 -0.35 0 -0.38
SCALE 0
PLANE X 0 1
CRPCIRC 1 10 9 0.503041 34.82 1
CRPCIRC 2 10 6 0.503041 55.18 1
CRPCIRC 3 10 11 0.503041 270 3
SCALE 0
PT 14 -0.5 0 -0.38
PT 15 -0.5 0.1505 0.1
PT 16 -0.5 -0.1505 0.1
CRPCIRC 6 14 15 0.503041 34.82 1
CRPCIRC 7 14 16 0.503041 55.18 1
CRPCIRC 8 14 17 0.503041 270 3
CT 1 0 0.15 5 6 7 8 9 10 0
RG 1 1 1 0
CRLINE 11 15 9
CRLINE 12 16 6
CRLINE 13 17 11
CRLINE 14 18 12
CRLINE 15 19 13
SF4CR 1 6 12 1 11 0
SF4CR 2 12 7 13 2 0
SF4CR 3 13 3 14 8 0
SF4CR 4 14 4 15 9 0
SF4CR 5 15 10 11 5 0
CRLINE 16 9 5
CRLINE 17 5 2
CRLINE 18 6 2
SF4CR 6 1 18 17 16 0
CRLINE 19 9 8
CRLINE 20 5 4
```

```
CRLINE 21 8 4
SF4CR 7 16 19 21 20 0
CRLINE 22 8 7
CRLINE 23 4 3
CRLINE 24 7 3
PT 20 0.35 0 -0.38
PLANE X 0 1
CRPCIRC 27 20 8 0.503041 34.82 1
SF4CR 8 27 24 23 21 0
CRLINE 25 6 7
CRLINE 26 2 3
SF4CR 9 18 26 24 25 0
SF4CR 10 17 20 23 26 0
CRPCIRC 28 20 7 0.503041 55.18 1
CRPCIRC 29 20 21 0.503041 270 3
CRLINE 32 9 6
PT 24 0.5 0 -0.38
PT 25 0.5 0.1505 0.1
PT 26 0.5 -0.1505 0.1
PLANE X 0 1
CRPCIRC 37 24 25 0.503041 34.82 1
CRPCIRC 38 24 26 0.503041 55.18 1
CRPCIRC 39 24 27 0.503041 270 3
CT 2 0 0.15 5 37 38 39 40 41 0
RG 2 1 2 0
CRLINE 42 8 25
CRLINE 43 7 26
SF4CR 13 42 37 43 27 0
CRLINE 44 21 27
SF4CR 14 43 38 44 28 0
CRLINE 45 22 28
SF4CR 15 29 44 39 45 0
CRLINE 46 23 29
SF4CR 16 45 40 46 30 0
SF4CR 17 46 41 42 31 0
CRLINE 47 11 21
CLS 1
SF4CR 18 2 47 28 25 0
CRLINE 48 12 22
SF4CR 19 3 47 29 48 0
CRLINE 49 13 23
SF4CR 20 4 48 30 49 0
SF4CR 21 5 49 31 19 0
PH 1 SF 1 0.1 0.0001 1
CLS 1
MA_PH 1 1 1
```

```
VIEW 0 0 1 0
VIEW 1 1 1 0
PSF 10 1 10 1 1 1 4
CLS 1
CLS 1
NTCR 26 1 26 1
NPCR 23 2 23 1
NJCR 20 3 20 1
QCR 17 4 17 1
CLS 1
```

Table 4.2 Listing of *figure6.in*

figure6.MOD	" Input file with node and element information"
figure6.out	" Output file with RCS as a function of look angle"
0.7,0.31	" x- and y- dimensions normalized with wavelength of rectangular cavity
0.1	length of cavity normalized with respect to wavelength
1	integer flag to consider higher order modes in the cavity
30	number of TE modes to be considered
30	number of TM modes to be considered
0	alpha = 0 for H-polarization (for E-polarization alpha =90)
0.,0.	theta and phi incident angles in degrees
1.,0	increment in theta and phi in degrees
30.	frequency in GHz
(1.,0.),(1.,0.)	complex relative permittivity and permeability of medium inside cavity

Table 4.3 Listing of *figure6.out*

```
X-dimension of WG =  0.7000000    wavelength
 Y-dimension of WG =  0.3100000    wavelength
 Length of WG cavity =  0.1000000    wavelength
 Number of waveguide modes =          60
 Number of Nodes Used =   552
 Number of Elements Used =     1100
 Frequency in Ghz =    30.00000
```

alpha	theta	phi	cross-pol	co-pol
0.	0.	0.	-5.933923	6.347271
0.	1.000000	0.	-5.935130	6.339834
0.	2.000000	0.	-5.946536	6.312681

0.	3.000000	0.	-5.968001	6.266007
0.	4.000000	0.	-5.999329	6.200232
0.	5.000000	0.	-6.040510	6.115752
0.	6.000000	0.	-6.091329	6.013002
0.	7.000000	0.	-6.151697	5.892314
0.	8.000000	0.	-6.221767	5.753819
0.	9.000000	0.	-6.301365	5.597322
0.	10.00000	0.	-6.390241	5.422188
--	-------	---	-------	--------
--	-------	--	------	--------
0.	174.0000	0.	-58.31413	4.871758
0.	175.0000	0.	-57.79329	5.028406
0.	176.0000	0.	-57.26915	5.159277
0.	177.0000	0.	-56.59153	5.262630
0.	178.0000	0.	-55.61058	5.337103
0.	179.0000	0.	-54.31091	5.381660
0.	180.0000	0.	-52.79220	5.395699

3.5 Example 5

In this example a rectangular aperture by backed by a rectangular cavity and placed along the circumference of a finite conducting circular cylinder, as shown in figure 7 is considered. *.SES, *. in, and *. out files used to run this case are shown in Tables 5.1, 5.2, and 5.3, respectively.

Table 5.1 Listing of *figure7.SES*

```
C*
C*  COSMOS/M      Geostar V1.70
C*  Problem : figure7          Date :  1-30-95  Time : 11:33:48
C*
C* FILE figure7.SES 1 1 1 1
PLANE Z 0 1
VIEW 0 0 1 0
PT 1 0 0 0
PT 2 -0.1505 -0.35 0
PT 3 0.1505 -0.35 0
PT 4 0.1505 0.35 0
PT 5 -0.1505 0.35 0
```

```
PT 6 -0.1505 -0.35 0.1
PT 7 0.1505 -0.35 0.1
PT 8 0.1505 0.35 0.1
PT 9 -0.1505 0.35 0.1
PT 10 -0.1505 0 -0.25
SCALE 0
VIEW 1 1 1 0
PLANE X 0 1
CRPCIRC 1 10 9 0.494975 90 1
CRPCIRC 2 10 6 0.494975 270 3
SCALE 0
PT 13 -0.1505 0 -0.25
PT 13 -0.5 0 -0.25
PT 14 -0.5 0.35 0.1
PT 15 -0.5 -0.35 0.1
CRPCIRC 5 13 14 0.494975 90 1
CRPCIRC 6 13 15 0.494975 270 3
SCALE 0
CT 1 0 0.1 4 5 6 7 8 0
RG 1 1 1 0
CRLINE 10 15 6
CRLINE 11 14 9
SF4CR 1 1 11 5 10 0
CRLINE 12 16 11
SF4CR 2 10 2 12 6 0
CRLINE 13 17 12
SF4CR 3 12 3 13 7 0
SF4CR 4 13 4 11 8 0
CRLINE 14 9 5
CRLINE 15 6 2
CRLINE 16 2 5
CRLINE 17 5 4
CRLINE 18 4 3
CRLINE 19 3 2
CRLINE 20 8 4
CRLINE 21 7 3
PT 18 0.1505 0 -0.25
CRPCIRC 22 18 8 0.494975 90 1
CRPCIRC 23 18 7 0.494975 270 3
CRLINE 26 9 8
CRLINE 27 12 20
SF4CR 5 26 25 27 4 0
CRLINE 28 11 19
SF4CR 6 27 24 28 3 0
CRLINE 29 6 7
SF4CR 7 28 23 29 2 0
```

```
SF4CR 9 1 14 16 15 0
SF4CR 10 26 20 17 14 0
SF4CR 11 22 21 18 20 0
SF4CR 12 29 21 19 15 0
SF4CR 13 16 19 18 17 0
PT 21 0.5 0 -0.25
PT 22 0.5 0.35 0.1
PT 23 0.5 -0.35 0.1
SCALE 0
CRPCIRC 30 21 22 0.494975 90 1
CRPCIRC 31 21 23 0.494975 270 3
CT 2 0 0.1 4 30 31 32 33 0
RG 2 1 2 0
CRLINE 34 8 22
CRLINE 35 7 23
SF4CR 14 34 30 35 22 0
CRLINE 36 19 24
SF4CR 15 35 31 36 23 0
CRLINE 37 20 25
SF4CR 16 36 32 37 24 0
SF4CR 17 37 33 34 25 0
PH 1 SF 1 0.1 0.0001 1
CLS 1
MA_PH 1 1 1
CLS 1
PSF 13 1 13 1 1 1 4
NTCR 19 1 19 1
NPCR 18 2 18 1
NJCR 17 3 17 1
QCR 16 4 16 1
```

Table 5.2 Listing of *figure7.in*

figure7.MOD	" Input file with node and element information"
figure7.out	" Output file with RCS as a function of look angle"
0.31,0.7	" x- and y- dimensions normalized with wavelength of rectangular cavity
0.1	length of cavity normalized with respect to wavelength
1	integer flag to consider higher order modes in the cavity
30	number of TE modes to be considered
30	number of TM modes to be considered
0	alpha = 0 for H-polarization (for E-polarization alpha =90)
0.,0.	theta and phi incident angles in degrees
1.,0	increment in theta and phi in degrees
30.	frequency in GHz
(1.,0.),(1.,0.)	complex relative permittivity and permeability of medium inside cavity

Table 5.3 Listing of *figure7.out*

X-dimension of WG = 0.31000000 wavelength
Y-dimension of WG = 0.700000 wavelength
Length of WG cavity = 0.1000000 wavelength
Number of waveguide modes = 60
Number of Nodes Used = 550
Number of Elements Used = 1096
Frequency in Ghz = 30.00000

alpha	theta	phi	cross-pol	co-pol
0.	0.	0.	-14.81105	6.143041
0.	1.000000	0.	-14.86441	6.125021
0.	2.000000	0.	-14.92570	6.073569
0.	3.000000	0.	-14.99266	5.989009
0.	4.000000	0.	-15.06429	5.871937
0.	5.000000	0.	-15.13739	5.723056
0.	6.000000	0.	-15.21013	5.543458
0.	7.000000	0.	-15.28020	5.334379
0.	8.000000	0.	-15.34564	5.097300
0.	9.000000	0.	-15.40529	4.833958
0.	10.00000	0.	-15.45568	4.546342
0.	11.00000	0.	-15.49823	4.236658
0.	12.00000	0.	-15.53147	3.907334
0.	13.00000	0.	-15.55477	3.560932
--	--------	--	---------	--------
--	--------	--	---------	--------
0.	172.0000	0.	-35.59557	4.241209
0.	173.0000	0.	-35.00657	4.387676
0.	174.0000	0.	-34.46977	4.516529
0.	175.0000	0.	-33.97979	4.627316
0.	176.0000	0.	-33.53917	4.719339
0.	177.0000	0.	-33.14160	4.791856
0.	178.0000	0.	-32.78939	4.844146
0.	179.0000	0.	-32.47799	4.875624
0.	180.0000	0.	-32.20755	4.885905

4. NUMERICAL RESULTS

To validate the present analysis and computer code, various numerical examples are considered. For validation, the numerical results obtained by ME-MoM are compared with results obtained by the hybrid Finite Element Method and Method of Moments (FEM-MoM) method. In the FEM-MoM method, EM fields inside the cavity are obtained using the Finite Element Method and the fields outside the cavity are obtained using the Method of Moments. The unknown fields are obtained by subjecting the total electric fields to appropriate boundary conditions. The results obtained by ME-MoM are also compared with the pure MoM approach. In the pure MoM approach, the inner wall of cavity along with the outer surface of the conducting body is considered as one closed 3D conducting surface. The Electric Field Integral Equation (EFIE) with electric surface current density as unknown is then obtained by subjecting the total tangential electric field on the entire closed surface to zero. The electric surface current density obtained after solving the EFIE is then used to determine scattering pattern of cavity backed aperture recessed in a 3D conducting body.

As a first example, the radar cross section of a rectangular cavity, as shown in figure 3, with dimensions a= 0.3 λ_0, b=0.3λ_0 and c = 0.2λ_0 is calculated. The cavity is assumed to be open at the z = 0 plane. For the numerical solution of equation (23), the infinite summations with respect to index p must be truncated to some finite number P, where P is the number of modes considered in ascending order of their cutoff frequencies. Numerical convergence of matrix equation (23) depends upon the choices of values of M, N, and P. For numerical convergence, sufficiently large values of M, N, and P must be selected. For $M = 42$, $N = 252$, and $P = 20$, the Radar Cross Section (RCS) of the rectangular cavity is calculated and presented in figure 3 along with the results obtained from the hybrid FEM-MoM. Further increases in values

M, N, and P were found to result in very insignificant changes in the RCS. The numerical results obtained using both methods agree very well verifying the validity of the combined field integral equation approach presented in this paper.

A second example considered for validation of the present approach is a rectangular cavity embedded in a solid conducting cubical box as shown in figure 4. The cavity dimensions are the same as described in figure 3. The cubical box with sides equal to 0.5 λ is considered. For $N = 300$, $M = 42$, and $P = 60$, the RCS pattern of the cavity embedded in a cubical solid box is calculated and presented in figure 4 along with the numerical results obtained using the pure MoM approach. In the pure MoM approach, the cubical box with the inner surface of cavity was considered as a closed conducting surface. From the plots in figure 4, it may be concluded that the results obtained by both methods agree well.

The present approach is also used to predict monostatic RCS's of cavities embedded in a finite metallic circular cylinder. In figure 5, a monostatic pattern of a rectangular cavity with dimensions $a = 0.3\lambda$, $b = 0.3\lambda$, and $c = 0.2\lambda$, which is embedded in one of the ends of the finite circular cylinder, is presented. The finite metallic cylinder is of length $L = 1\lambda$ and diameter $r = 0.5\lambda$. The monostatic pattern of the cavity is also calculated using the pure MoM approach and is presented in figure 5. The results obtained by both methods agree well.

To demonstrate the application of the present approach to a cavity backed aperture mounted on curve surfaces, a rectangular cavity with x width equal to 0.7λ, y width equal to 0.31λ, and z depth equal to 0.2λ embedded in the finite metallic cylinder as shown in figure 6 is considered. To be able to match the cavity modal fields with electromagnetic fields outside the cavity across the cavity aperture, the aperture surface must be planar and normal to z-axis. However, for the example shown in figure 6 the aperture plane is not planar. To avoid this difficulty for apertures on curve surfaces, the equivalent cavity aperture which is a little inside the curved surface is considered for matching fields across the cavity aperture. For the example under consideration, the cavity aperture at $z = -0.1\lambda$ is considered. The monostatic pattern of the cavity mounted on cylindrical surface calculated using the present method and the pure MoM method is shown in figure 6. There is good agreement between the two results.

Monostatic patterns of a rectangular cavity with longer dimension along the circumferential direction of a finite metallic cylinder are calculated using the present method and the pure MoM technique. The results are presented in figure 7. For these results, a rectangular cavity with x width equal to 0.31λ , y width equal to 0.7λ, and z depth equal to 0.2λ embedded in a finite metallic cylinder of length L equal to 1.0λ and the diameter r equal to 0.5λ was considered. The results obtained by both methods agree well with little disagreement near broad side angles.

5. CONCLUSION

The problem of electromagnetic scattering from a cavity backed aperture recessed in a 3D conducting body has been analyzed using the combined field integral equation approach. The EM fields outside the cavity are obtained in terms of the free space Green's function and electric and magnetic surface current densities present on the surface of conducting bodies including the aperture. The EM fields inside the cavity are obatined in terms of cavity modal functions. The combined field integral equations are then derived by subjecting the electric and magnetic fields to appropriate boundary conditions. Using the Method of Moments, the integral equations are solved for unknown surface current densities. The scattering characteristic of the cavity backed aperture is then determined from the surface current densities. The numerical results obtained by the present method are compared with the numerical results obtained by FEM-MoM and the pure MoM methods. The computed results for the rectangualr cavities considered in this paper agree well with the results obtained by the hybrid FEM-MoM and the pure MoM methods. The limitation of the present method is that it can be used to analyze regularly shaped cavities filled with homogeneous material.

REFERENCES

[1] D. T. Auckland and R. F. Harrington, " Electromagnetic transmission through a filled slit in a conducting plane of finite thickness, TE case," IEEE Trans. on Microwave Theory & Tech., Vol. MTT-26, pp. 499-505, July 1978.

[2] D. T. Auckland and R. F. Harrington, " A nonmodal formulation for electromagnetic transmission through a filled slot of arbitrary cross-section in a thick conducting screen," IEEE Trans. on Microwave Theory & Tech., Vol. MTT-28, pp. 548-555, June 1980

[3] R. F. Harrington and J. R. Mautz, "A generalized network formulation for aperture problems," IEEE Trans. on Antennas and Propagation, Vol. AP-24, pp. 870-873, Nov. 1976.

[4] J. R. Butler, Y. Rahmat-Samii, and R. Mitra, "Electromagnetic penetration through apertures in conducting surfaces," IEEE Trans. on Antennas and Propagation, Vol. AP-26, pp. 82-93, Jan. 1978.

[5] J. M. Jin, and J. L. Volakis, " TE scattering by an inhomogeneously filled aperture in a thick conducting plane," IEEE Trans. on Antennas and Propagation, Vol. AP-38, 1990.

[6] J. M. Jin, and J. L. Volakis, " A finite element boundary integral formulation for scattering by three dimensional cavity backed apertures," IEEE Trans.. on Antennas and Propagation, Vol. AP-39, Jan. 1991.

[7] Barkeshli K., and Volakis J. L., “ TE scattering by a two dimensional groove in a ground plane using higher order boundary conditions,” IEEE Trans. on Antennas and Propagation, Vol. AP-38, Oct. 1990.

[8] K. Barkeshli., and J. L. Volakis, “ Electromagnetic scattering from an aperture formed by a rectangular cavity recessed in a ground plane,” Journal of Electromagnetic Waves and Applications, Vol. No. 7, pp. 715-734, 1991.

[9] E. Heyman, et al, “ Ray-mode analysis of complex resonances of an open cavity,” Proc. IEEE, Vol. 77, no. 5, pp. 780-787, May 1989.

[10] P. K. Pathak and R. J. Buckholder, “ Modal, ray, and beam techniques for analyzing the EM scattering by open ended waveguide cavities,” IEEE Trans. on Antennas and propagation, Vol. AP-37, no. 5, pp. 635-647, May 1989.

[11] H. Ling, S. W. Lee, and R. C. Chou, “ High-frequency RCS of open cavities with recangular and circular cross sections,” IEEE Trans. on Antennas and Propagation, Vol. AP-37, No. 5, pp. 648-654, May 1989.

[12] L. N. Medyesi-Mitschang, and C. Eftimiu, “Scattering from wires and open circular cylinders of finite length using entire domain Galerkin expansions,” IEEE Trans. on Antennas and Propagation, Vol. AP-30, No. 4, pp. 628-636, July 1982.

[13] P. L. Huddleston, “ Scattering from conducting finite cylinders with thin coatings,” IEEE Trans. on Antennas and Propagation, Vol. AP-35, No. 10, pp. 1128-1134, Oct., 1987.

[14] S. M. Rao, D. R. Wilton, and A. W. Glisson, “ Electromagnetic scattering by surfaces of arbitrary shape,” IEEE Trans. on Antennas and Propagation, Vol. AP-30, pp. 409-418, May 1982.

[15] R. F. Harrington, *Time Harmonic Electromagntic Fields*, McGraw-Hill Book Company, 1961.

[16] O. C. Zienkiewicz, *The Finite Elements Method in Engineering Science,* McGraw-Hill Book Company, London, England, 1971.

{17] D. R. Wilton, et al., " Potential integrals for uniform and linear source distributions on polygonal and polyhedral domains," IEEE Trans. on Antennas and Propagation, Vol. AP-32, pp. 276-281, March 1984.

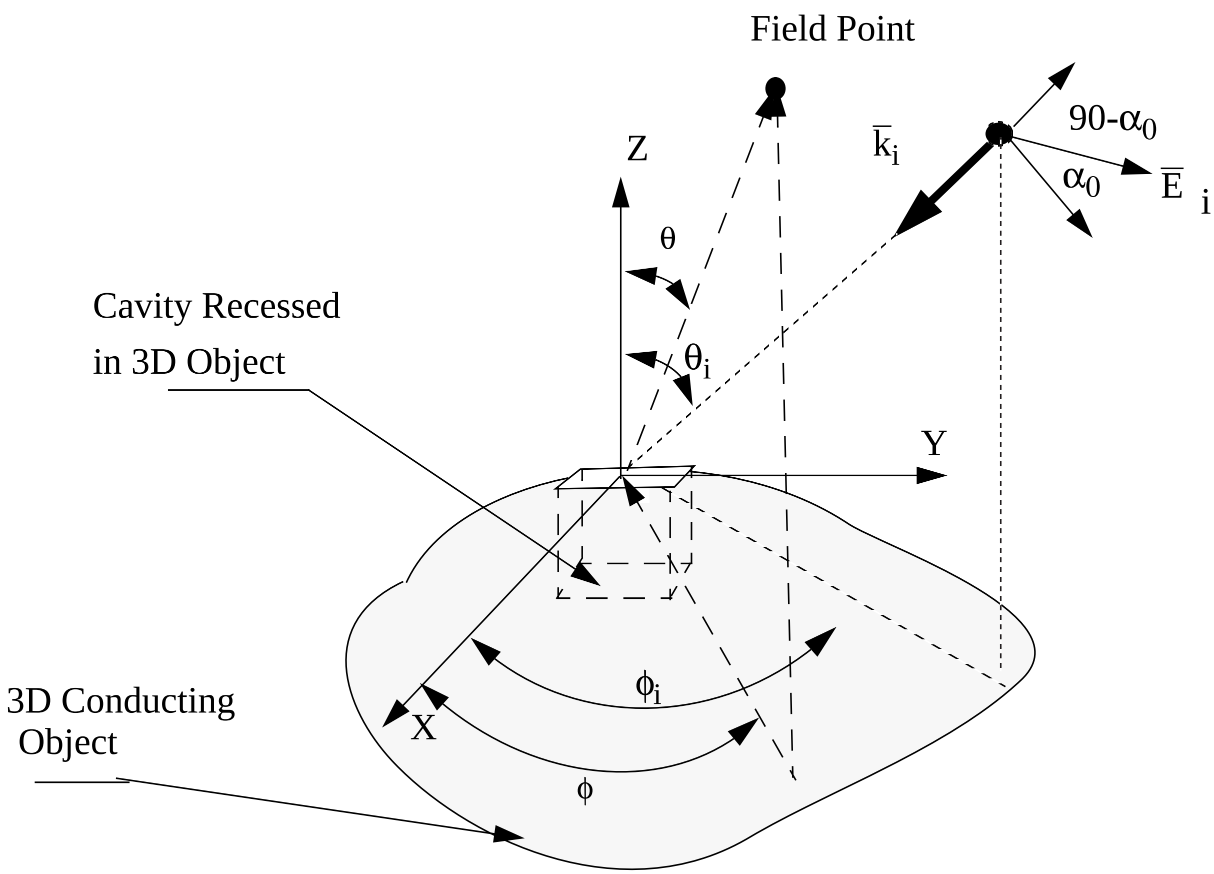

Figure 1 An open ended rectangular cavity recessed in a 3D conducting surfac
and illuminated by a plane wave.

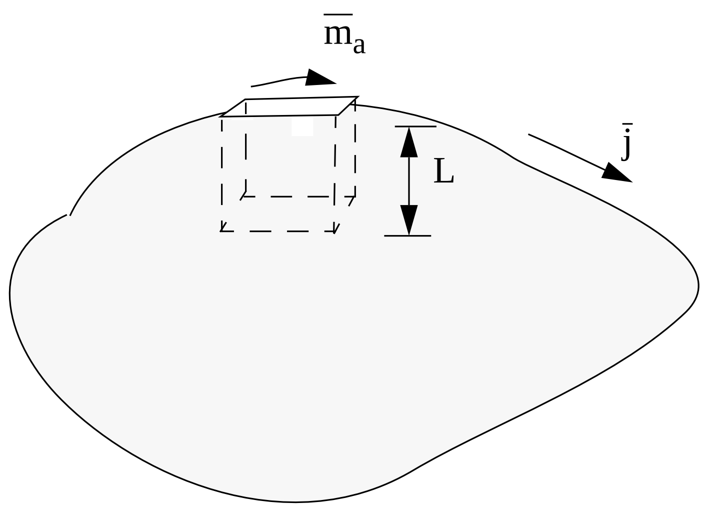

Figure 2 Equivalent electric and magnetic surface currents

Figure 3

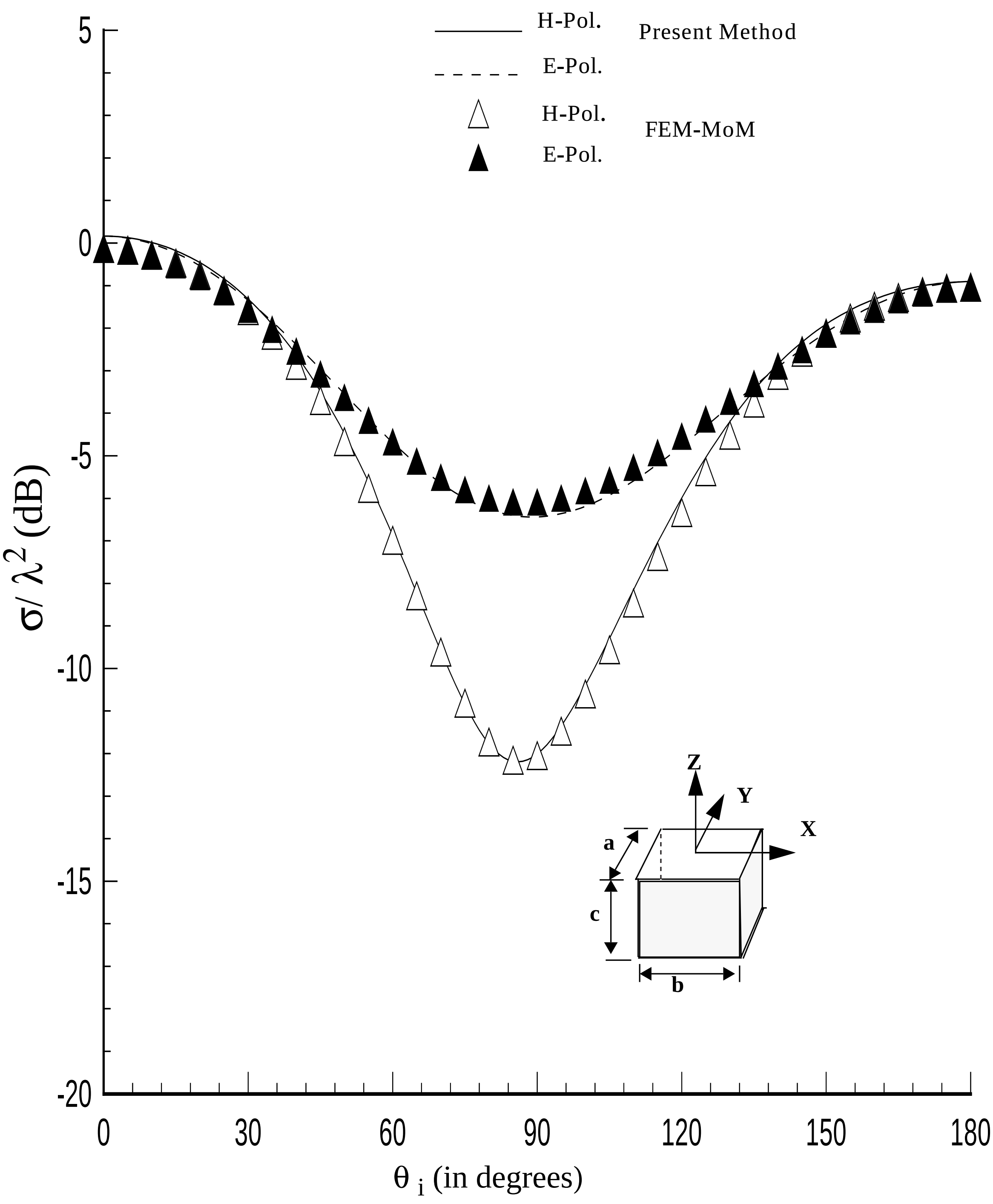

Figure 3 Backscatter RCS patterns for a rectangular cavity as shown with dimensions a=0.3 λ , b= 0.3 λ , c= 0.2 λ without a ground plane for E- and H- polarized incident plane wave. Solid and hollow triangles indicate numerical data obtained using FEM-MoM

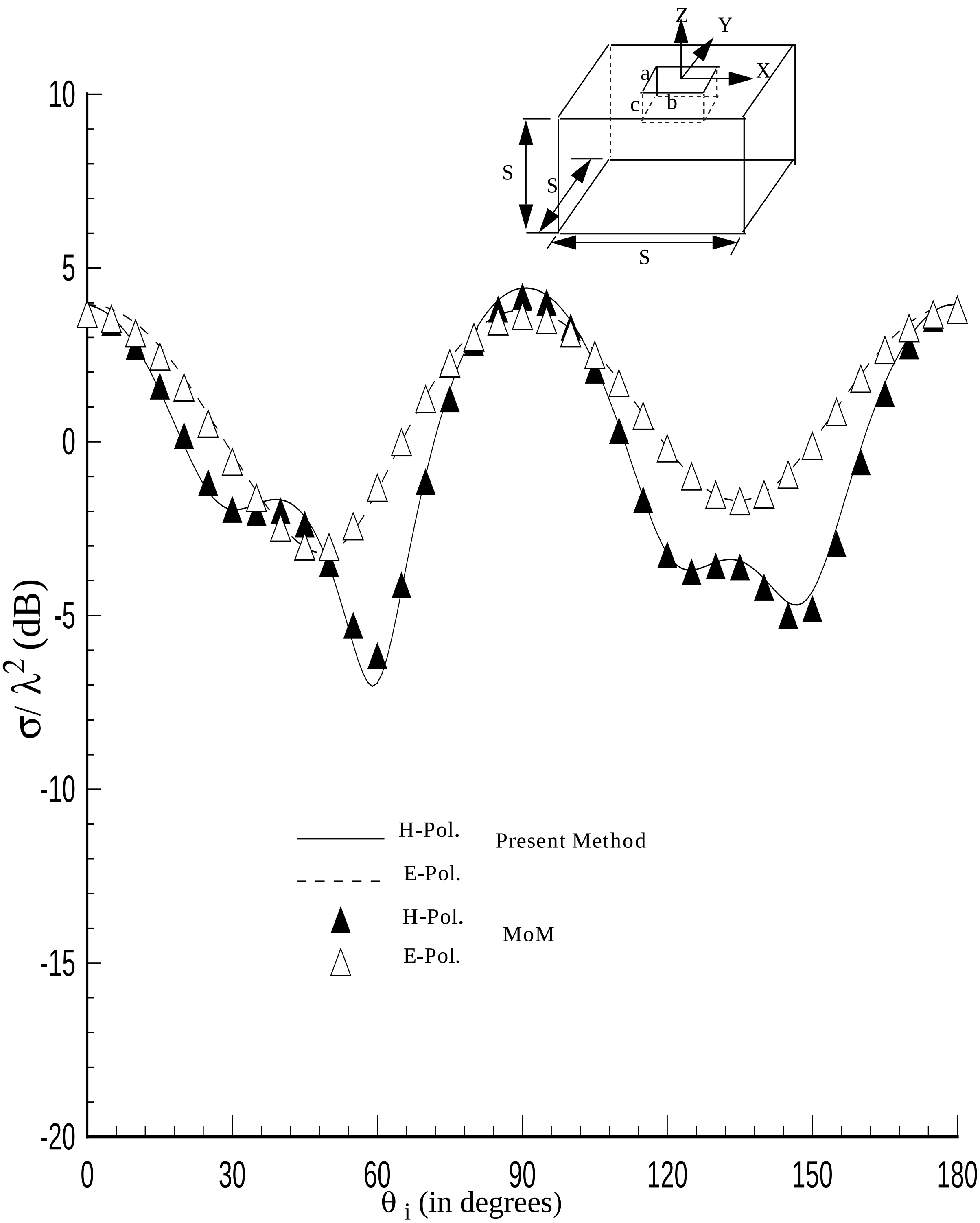

Figure 4 Backscatter RCS patterns for a rectangular cavity (a=0.3 λ , b=0.3 λ, c=0.2λ) embedded in a solid cube with side S =0.5 λ , as shown for E- and H-polarized plane wave incidenc ($\phi_i = 0^0$). Solid and hollow triangles indicate results obtained by the method of moments.

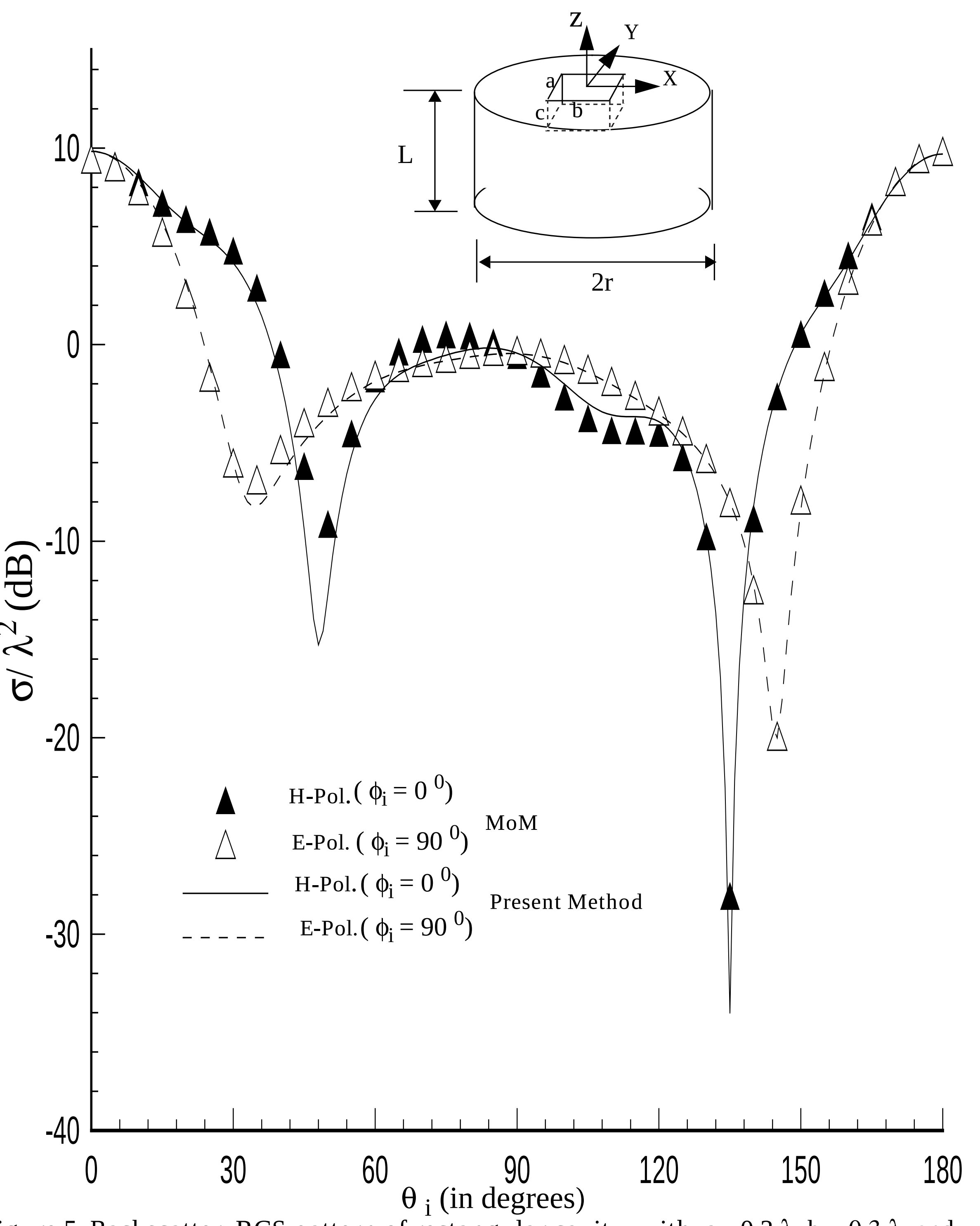

Figure 5 Backscatter RCS pattern of rectangular cavity with a= 0.3 λ, b = 0.3 λ, and c = 0.2 λ embedded in a conducting circular cylinder as shown with L =0.5 λ and r = 0.5 λ.

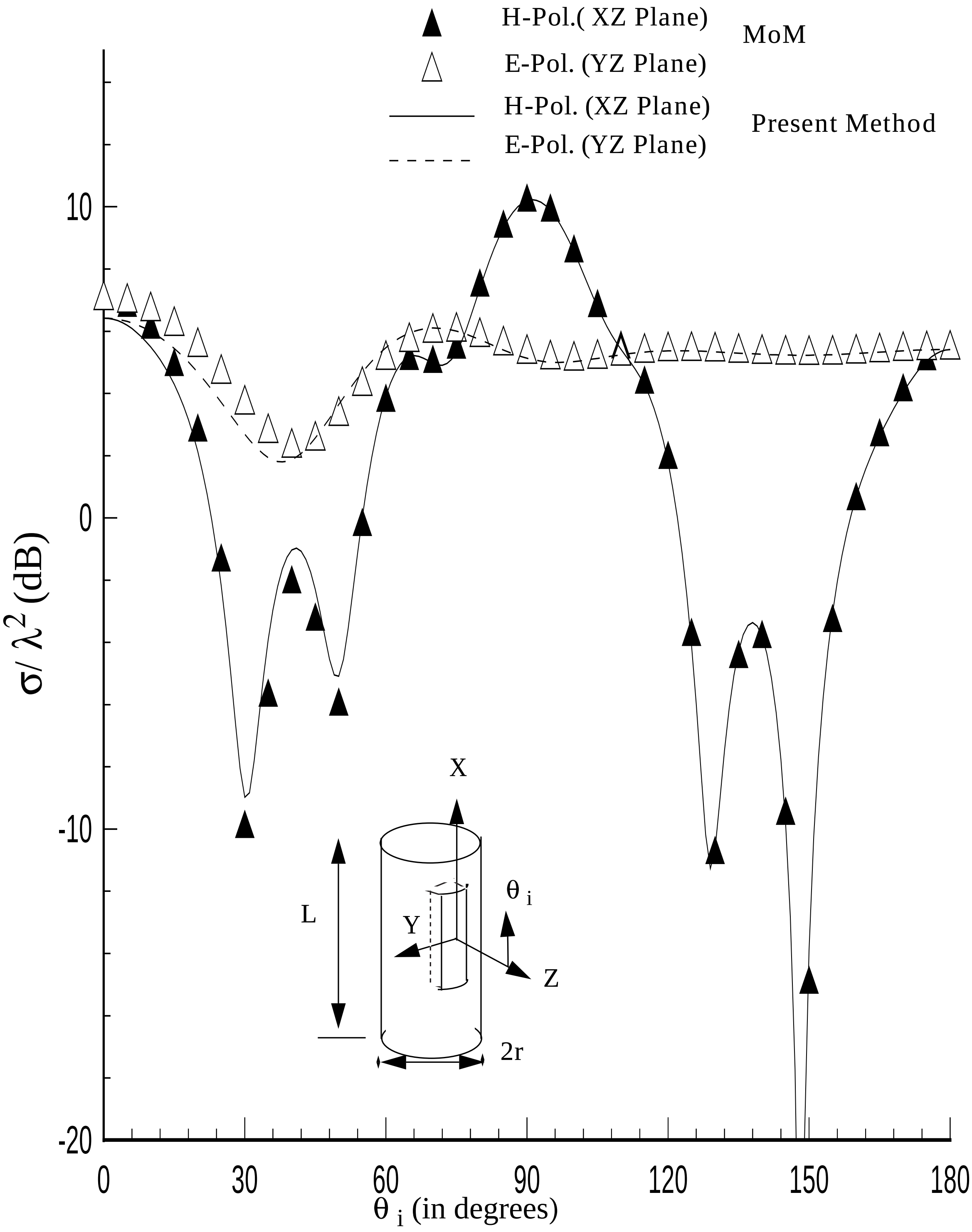

Figure 6 Backscatter RCS pattern of rectangular cavity with x width = 0.7 λ, y width 0.31 λ, and depth = 0.2 λ, embedded in a conducting circular cylinder with L = 1 λ, r = 0.5 λ.

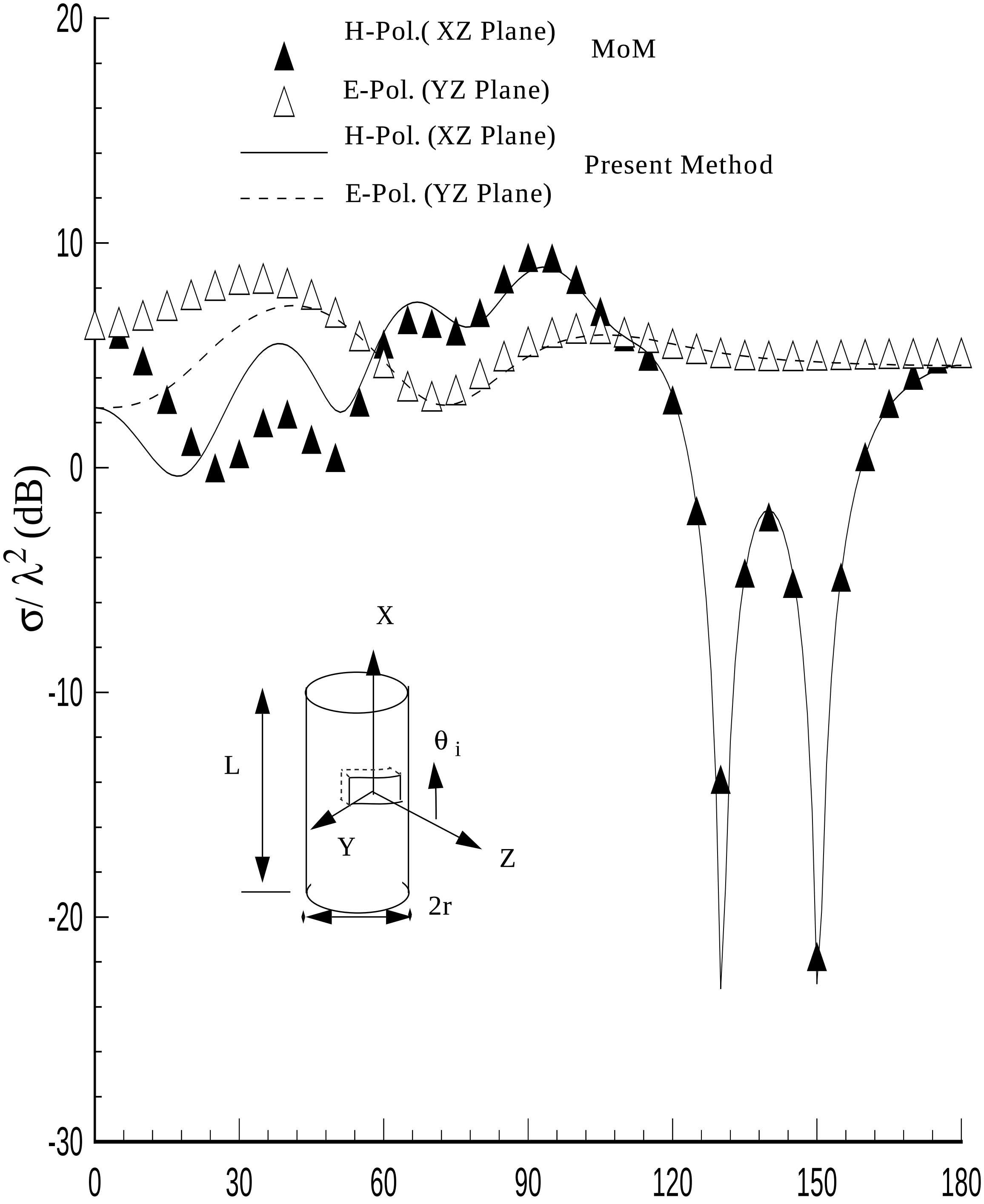

Figure 7 Backscatter RCS pattern of rectangular cavity with x width = 0.31 λ, y width =0.7λ, and depth = 0.2 λ embedded in a conducting circular cylinder with L = 1.0λ and r = 0.5λ.